2D Materials

RECEIVED
13 March 2015

REVISED
19 May 2015

ACCEPTED FOR PUBLICATION
29 June 2015

PUBLISHED
30 July 2015

PAPER

Threshold and efficiency for perforation of 1 nm thick carbon nanomembranes with slow highly charged ions

Richard A Wilhelm[1], Elisabeth Gruber[2], Robert Ritter[2], René Heller[1], André Beyer[3], Andrey Turchanin[4], Nico Klingner[1], René Hübner[1], Michael Stöger-Pollach[5], Henning Vieker[3,6], Gregor Hlawacek[1], Armin Gölzhäuser[3], Stefan Facsko[1] and Friedrich Aumayr[2]

[1] Helmholtz-Zentrum Dresden-Rossendorf, Institute of Ion Beam Physics and Materials Research, 01328 Dresden, Germany
[2] TU Wien, Institute of Applied Physics, 1040 Vienna, Austria
[3] Bielefeld University, Faculty of Physics, 33615 Bielefeld, Germany
[4] Friedrich Schiller University Jena, Institute of Physical Chemistry, 07743 Jena, Germany
[5] TU Wien, USTEM, 1040 Vienna, Austria
[6] Current address: CNM Technologies, Brökerstr. 8, 33602 Bielefeld, Germany

E-mail: r.wilhelm@hzdr.de

Keywords: CNM, SAM, membrane, slow highly charged ion

Supplementary material for this article is available online

Abstract

Cross-linking of a self-assembled monolayer of 1,1′-biphenyl-4-thiol by low energy electron irradiation leads to the formation of a carbon nanomembrane, that is only 1 nm thick. Here we study the perforation of these freestanding membranes by slow highly charged ion irradiation with respect to the pore formation yield. It is found that a threshold in potential energy of the highly charged ions of about 10 keV must be exceeded in order to form round pores with tunable diameters in the range of 5–15 nm. Above this energy threshold, the efficiency for a single ion to form a pore increases from 70% to nearly 100% with increasing charge. These findings are verified by two independent methods, namely the analysis of individual membranes stacked together during irradiation and the detailed analysis of exit charge state spectra utilizing an electrostatic analyzer.

Carbon nanomembranes (CNMs) made from self-assembled monolayers of different aromatic molecules are a novel type of ultrathin material that shows high stiffness with a Young's modulus of about 10 GPa [1]. CNMs are also easily chemically modified [2] and may therefore serve as a functional two-dimensional material. The formation of CNMs involves the cross-linking of a self-assembled monolayer of aromatic molecules by low energy electron or UV–light irradiation. The choice of aromatic molecules finally determines the thickness of the membrane in the range of 0.6nm (naphthalene, NPHT) to 2.2 nm (hexa-*peri*-benzocoronene, HBC-CN) [3]. Even more remarkable CNM can be transformed into a single layer graphene sheet by thermal decomposition at about 800 °C in vacuum or under protective atmosphere [4]. To integrate these membranes in devices they may be structured in a desired way by means of lithographic methods [2]. Since these membranes are typically insulating in their pristine state, they are susceptible to lithography by electronic excitations, i.e., electron beams, lasers, or even highly charged ions (HCI).

Typical ion beam lithography methods require large fluencies to achieve a desired material modification. When swift heavy ions [5, 6] or slow HCI [7, 8] are used instead, a single ion impact can already lead to dramatic changes in the solid that can be of interest for technological applications [9–11]. Considering the depth distribution of damage induced by these classes of ions, slow HCI are preferred for surface-only modification due to the deposition of their potential energy in a shallow region below the surface [12, 13]. The potential energy of the HCI is defined as the sum of the binding energies of all removed electrons. Several studies showed that HCI may lead to a variety of different nanostructure types, such as pit-like structures with very large corresponding sputter yields [14], nanometer-sized protrusions called hillocks from the surface [8, 15–17], crater structures [18, 19], or even solely changes in the local density of states [20–23]

depending on the target material. By reducing the solid's thickness to the range of the potential energy deposition depth (typically a few nm) nanopores can also be created [24] and may be used as molecular sieves [25, 26].

Here we investigate the perforation of 1 nm thick freestanding CNMs by impacts of single, slow HCI. Extending our recent study [24] on the formation of nanopores in these membranes to a wider range of kinetic and potential energies and comparing with the data obtained from transmitted ions we are able to draw a phase diagram for CNM nanostructuring by slow HCI. Furthermore, we investigate the reported potential energy threshold for perforation in more detail.

HCI were produced in a room-temperature electron beam ion trap [27] that is a part of the Two-Source-Facility of the Ion Beam Center at the Helmholtz-Zentrum Dresden-Rossendorf. HCI were extracted at a constant acceleration voltage of 4.4 kV resulting in an initial kinetic ion energy of 4.4 keV·Q, where Q is the ion's charge state. The ion beam was charge state separated by an analyzing magnet and focused on the target by an assembly of electrostatic lenses. An adjustable voltage difference between the beam-line (including the ion source) and the target chamber allowed the deceleration of the ions to a few keV (few 100 V·Q) final kinetic energy. A CNM was mounted on a transmission electron microscopy (TEM) grid suspended inside the target chamber (see details next). An electrostatic analyzer was mounted behind the grid, which allowed the determination of the charge state distribution and the corresponding energies of the transmitted ions. The base pressure inside the target chamber was in the range of 10^{-9} mbar.

Irradiated samples were transferred to air and transported either to an aberration corrected FEI TITAN 80–300 TEM operated at 300 keV or to a ZEISS Orion Nanofab helium ion microscope (both located at the Ion Beam Center) for imaging. Since microscopy analysis on these samples is very time consuming, some samples were sent to the University of Bielefeld and analyzed with a ZEISS OrionPlus HIM and others to the USTEM TU Wien and imaged with a FEI TECNAI F20 TEM at 200 keV electron energy to divide rare measurement time. Some samples were analyzed at different facilities, whereas the results did not depend on the type of machine used for analysis.

The CNMs used here were produced by low energy electron irradiation (cross-linking) of a self-assembled monolayer of 1,1′-biphenyl-4-thiol (BPT, $(C_6H_5)_2$ SH) grown on a metal substrate (for details see [28, 29]). The fully cross-linked monolayer was released from the growth substrate and transferred onto a TEM grid with an underlying holey- or lacey-carbon support film (both delivered from Plano GmbH, Germany) for enhanced mechanical stability [30]. The CNM spans over micrometer-sized holes in the carbon support film and is freestanding. The thickness of the CNM is determined by the height of the BPT monolayer and corresponds well to 1nm [1, 30]. From the process of cross-linking we assume that a large amount of (if not all) hydrogen bonds are cleaved within the BPT molecules. Additional Auger electron spectroscopy analysis excludes the presence of heavy elements above a concentration of 1 at%. Thus the CNM is treated as pure amorphous carbon material. The CNMs were used as supplied without any further treatment (no annealing).

In the first step, individual CNMs were irradiated with Xe ions at charge states ranging from Q = 20–40 and kinetic energies from about 2 keV to 180 keV. Applied fluencies were in the range of 5×10^9 cm^{-2} to 5×10^{10} cm^{-2} for all experiments, resulting in 50–500 ion impacts per μm^2. For high ion charge states, nanopores in the membranes were observed with round shape and diameters in the range of a few nm, which are randomly distributed in the CNM (see figure 1). We attribute each observed nanopore to a single ion impact because the probability of double impact is negligible at the fluencies applied.

A detailed study of the size dependence of the nanopores on ion's potential energy and imaging methods was published recently [24] and is now extended. Figure 2 shows a phase diagram, i.e. combinations of kinetic and potential energies of the ions where nanopores were created (green dots). Combinations where no nanopores could be found are marked as red squares. The threshold in potential energy for nanostructuring the membranes is at about 10–12 keV ($Q \approx 28$). A weak dependence of the threshold on kinetic energy can also be observed in figure 2. The fact that a charge state or potential energy threshold exists for solid surface nanostructuring is a common phenomenon for slow HCI [7]. However, in the case of 1nm thick CNM, it could be shown that HCI at keV kinetic energies are not completely neutralized, thus only a fraction of the potential energy is deposited in the membrane [31]. In order to determine the amount of deposited potential energy per ion two independent methods were used. Besides the analysis of the transmitted ion beam with an electrostatic analyzer, as mentioned in the experimental section and in a recent publication [31], we also used a stack of three CNMs mounted on individual TEM grids (without holey- or lacey-carbon support) and squeezed together in one scanning electron microscopy holder. By irradiating this stack of CNMs and imaging each layer in the stack independently, indirect access to the exit charge state distribution of each layer and the pore formation efficiency could be obtained. The key difference from direct transmission measurements is that the electrostatic analyzer covers only a small solid angle in the forward direction and thus ions scattered out of the acceptance angle of the analyzer are not measured. To measure the total exit charge state distribution and determine the pore formation efficiency,

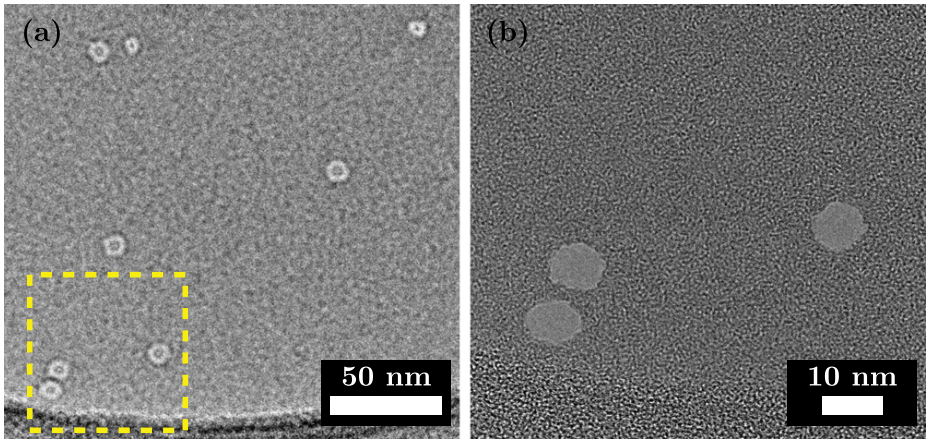

Figure 1. TEM images of a CNM irradiated with 176 keV Xe^{40+} ions. Left side (a) shows holes as bright spots, where the TEM was operated in underfocus to enhance contrast. The lower part of this image shows the holey-carbon support film as a darker area. The area inside the yellow square is shown with adjusted focus on the right side (b).

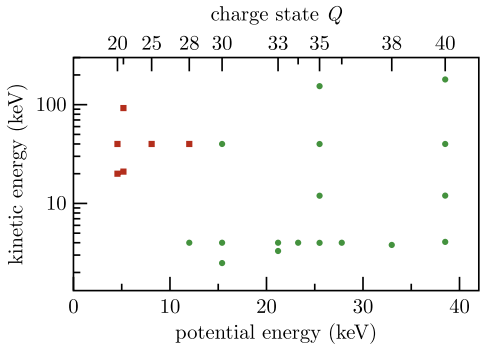

Figure 2. Phase diagram for pore formation by HCI on CNM. Green dots represent combinations of kinetic and potential energy where pores were observed and red squares where no pores were detected. The potential energy threshold is estimated at about 10 keV.

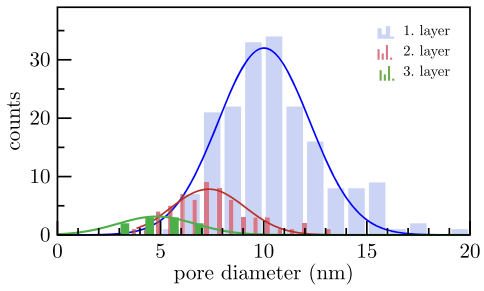

Figure 3. Histograms for pore sizes obtained from different CNM in a stack of three. The stack was irradiated with 40 keV Xe^{35+} ions. The mean and width of the distributions were extracted from a Gaussian fit. The bin widths are different for better representation.

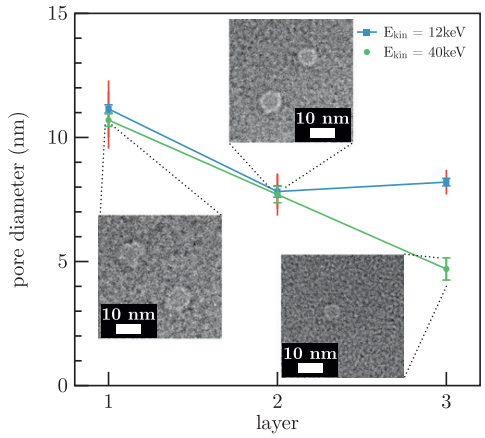

Figure 4. Mean pore sizes in each layer for two different stacks of three CNMs. The red bars represent the width of each distribution (standard deviation σ) and the error bars the uncertainty of the mean ($3 \times \sigma/\sqrt{n}$).

angle resolved measurements and subsequent integration of all the data are needed.

Irradiated layers of a stack of three CNMs were analyzed with TEM and helium ion microscopy (HIM). Surprisingly, pores could be observed not only in the first and second layer, but even in the third layer. Figure 3 shows the pore size distribution for each layer of a stack of CNM irradiated with 40 keV Xe^{35+} ions. A mean pore size of 10 nm was found in the first layer (blue) and the size decreases for increasing layer number. It should be noted that each data set in figure 3 was obtained from a different number of images. Figure 4 shows data from two different stacks. Both stacks were irradiated with Xe^{35+} ions at different kinetic energies of 12 keV (blue squares) and 40 keV (green dots).

Figure 5 shows an estimated pore density for the two stacks in figure 4. The pore density was calculated by dividing the total number of imaged pores by the total area of all images for that layer. By doing so we obtain an upper limit for the pore density, because areas where the pore density may be significantly lower were not imaged. Note that a typical TEM or HIM image has a field of view of $100 \times 100\ nm^2$ to $500 \times 500\ nm^2$ in order to observe small pores. In both

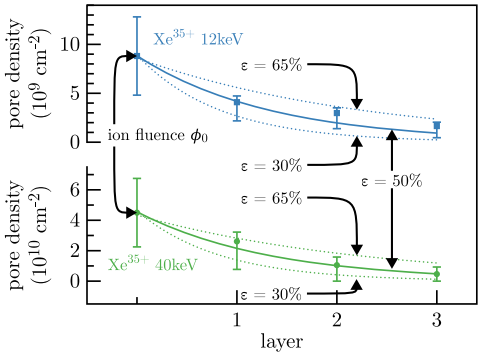

Figure 5. Pore density per layer for two different stacks of three CNMs. The data points were fitted by an exponential function $\phi_0 \cdot \varepsilon^L$, where ϕ_0 is the applied ion fluence (shown as a data point at $L = 0$). An efficiency ε of 50% yielded the best fit, whereas fits for efficiencies ε = 30% and 65% are indicated as dotted lines.

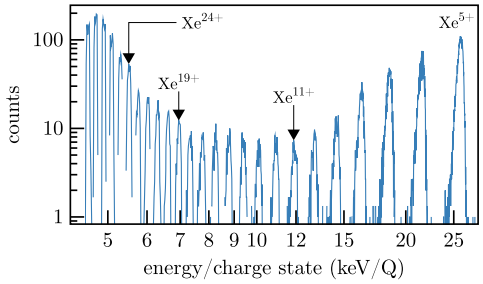

Figure 6. Typical transmission spectrum for highly charged Xe ions (here Q_{in} = 30) through a CNM. Ions in the transmitted charge state Q = 30 are not shown, because they result mainly from transmission through large cracks in the membrane.

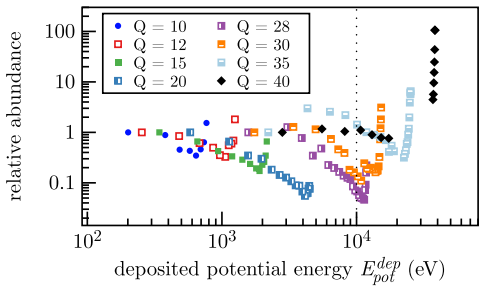

Figure 7. Relative abundance of deposited potential energy for Xe ions of different charge states at kinetic energies of 4.4 keV ·Q transmitted through a CNM. The potential energy threshold from figure 2 is shown as a vertical dotted line at 10 keV.

cases the first layer showed a pore density that is in fair agreement with the applied ion fluence. The ion fluence was determined by measuring the ion (electrical) current on the target holder (without secondary electron suppression) and estimating the beam spot size by moving a pin hole in the target holder over the beam spot. Thus, the ion fluence is affected by significant uncertainties (relativ uncertainty ≈50%). Considering this fact and the limitations in statistical averaging over a large number of pores and imaged areas, our previous statement [24] about *excellent* agreement of the pore density with ion fluence is probably too strong. From figure 5 a decrease of pore density per layer can be observed, as already indicated in figure 3 for both kinetic energies. Both data sets were fitted with a function $\varrho_A(L) = \phi_0 \cdot \varepsilon^L$, where ϕ_0 is—within the uncertainties discussed previously—the applied ion fluence, L denotes the layer number and ε the pore formation efficiency. The best fit for the efficiency is in both cases ε = 50%. The fit indicates that (for E_{kin} = 10–40 keV) at least 50% of the ions produce a pore upon impact. Fits with assumed efficiencies ε of 30% and 65% are plotted as dotted curves and yield an uncertainty estimate for the efficiency. Note that an ion cannot produce a pore in more than one layer due to the high corresponding sputter yields of a few 1000 atoms. Considering typical binding energies of a few eV per atom the main fraction of the potential energy is already consumed by one pore formation. Hence, the findings indicate that the transmission through each layer leads to a bimodal exit charge state distribution. One part of the ions is transmitted in low charge states ($Q \ll 28$)due to the energy deposition upon pore formation. The other part of the ions is still in sufficiently high charge states ($Q > 28$) enabling pore formation in the second layer. This observation is consistent with direct transmission measurements published recently [31].

Alternatively the pore formation yield can be deduced from charge state spectra of the transmitted ion beam. Transmission spectra were obtained for ions in different incident charge states Q_{in} and the maximal available kinetic energy of 4.4 keV·Q_{in} (for an example, see figure 6). From each spectrum the relative abundance of each exit charge state was extracted and is shown in figure 7 as a function of the deposited potential energy. (Note that the kinetic energies are different for each incident charge state.) To extract the correct abundances the data were deconvoluted from an artificial peak broadening by the electrostatic analyzer. A detailed description can be found in the Supporting Information. The deposited potential energy is $E_{pot}^{dep}(Q_{in}, Q_{out}) = E_{pot}(Q_{in}) - E_{pot}(Q_{out})$, i.e. the difference of potential energy of the incident and outgoing charge states. A fraction of this deposited potential energy may be lost by emission of energetic secondary electrons and photons and may therefore not be available to the pore formation process. Bodewitz *et al* showed recently that energetic electron emission originates also from within the material and thus potential energy deposition occurs below the surface as well [32]. The bimodal exit charge state distribution found in transmission measurements is characterized

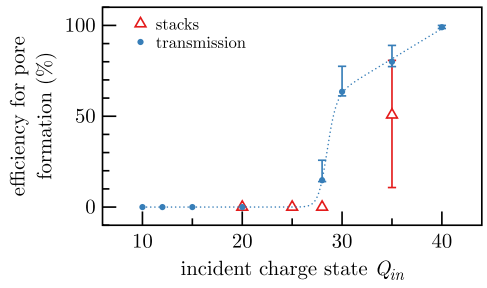

Figure 8. Efficiency for pore formation as a function of incident charge state and E_{kin} of 4.4 keV ·Q ions estimated from transmission data shown in figure 7 (blue dots) and from stack analysis (red triangles). The efficiency from transmission is a lower estimate, because the data in figure 7 does not contain ions with charge loss larger than 85%, i.e., single charged and neutral particles. In addition only ions transmitted in straight forward direction are accessible in the measurement.

in figure 7 by the minimum for each data set. High relative abundance for small E_{pot}^{dep} (left of the minimum) corresponds to high exit charge states and high relative abundance for larger E_{pot}^{dep} (right of the minimum) corresponds to low exit charge states. It should be noted here that due to experimental limitations (spectrometer voltage) the smallest observable exit charge state is $0.15 \cdot Q_{in}$. This means that for each set of data in figure 7, points with high relative abundance at the highest E_{pot}^{dep} are missing because neutral and almost neutral particles could not be measured.

However, by combining the empirical finding of figure 2 that the potential energy should be larger than about 10 keV in order to form pores in CNM and the relative abundance of potential energy deposition with values larger than 10 keV from figure 7 (threshold marked by the dotted line) we can directly estimate a pore formation efficiency. Figure 8 shows the efficiency per ion to form a pore as a function of the incident charge state and kinetic energies of 4.4 keV·Q_{in}. The values of efficiency are given by the quotient of the summed abundance of $E_{pot}^{dep} > 10$ keV and the summed abundance of all transmitted ions. The efficiency is 0 up to around $Q_{in} = 28$ and increases rapidly to about 70% at $Q = 30$. The rapid increase is again evidence that the threshold for nanostructuring of surfaces and membranes is sharp in terms of potential energy. For even larger charge states the efficiency increases linearly with charge state and reaches about 100% for $Q = 40$. Additionally the deduced efficiencies estimated from the stack experiments are shown as red triangles. Data for $Q < 30$ is taken from single layer irradiations where no pores were observed at 40 keV kinetic energy (see figure 2).

To estimate the importance of the potential energy in the sputter process the observed sputter yield may be compared to values obtained from a standard binary collision approximation simulation (TRIM). The sputter yield deduced from this simulation results exclusively from elastic collisions and is about three orders of magnitude below the observed yield. Even for a charge state enhanced nuclear scattering cross-section [33] the sputter yield from elastic collisions may not increase significantly due to the small thickness of the membrane and preferred forward scattering of heavy xenon projectiles on light carbon atoms. Thus, the potential energy is the driving force for the sputtering from the CNM together with possible enhanced *electronic* losses. Kinetically assisted potential sputtering was recently observed on a polymer—namely PMMA [34]—and alkali halides such as KBr [14], where also some contribution of kinetic losses to electronic excitations may be assumed. Finally, the role of the kinetic energy deposition in the pore formation process is not entirely clear, limiting the interaction time on the one hand but delivers energy to the nuclear and possibly to the electronic system on the other hand.

In this paper we showed that single slow HCI can be used to perforate CNMs with an efficiency of close to 100% when the ion's charge state is considerably higher than a threshold value of about $Q_{th} = 28$. This information can be derived from direct transmission measurements and independently from imaging a stack of several irradiated layers of CNM. It is shown that directly from charge exchange measurements information about structural changes in a material can be gained.

Acknowledgments

Financial support from the Deutsche Forschungsgemeinschaft (DFG) (project no. HE 6174/1-1) and from the Austrian FWF (project no. I 1114-N20) is acknowledged.

References

[1] Turchanin A and Gölzhäuser A 2012 *Prog. Surf. Sci.* **87** 108–62
[2] Beyer A, Godt A, Amin I, Nottbohm C T, Schmidt C, Zhao J and Gölzhäuser A 2008 *Phys. Chem. Chem. Phys.* **10** 7233–38
[3] Angelova P *et al* 2013 *ACS Nano* **7** 6489–97
[4] Matei D G *et al* 2013 *Adv. Mater.* **25** 4146–51
[5] Khalfaoui N, Rotaru C C, Bouffard S, Toulemond M, Stoquert J P, Haas F, Trautmann C, Jensen J and Dunlop A 2005 *Nucl. Instum. Methods. Phys. Res.* B **240** 819–28
[6] Ochedowski O, Osmani O, Schade M, Bussmann B K, Ban-d'Etat B, Lebius H and Schleberger M 2014 *Nat. Commun.* **5** 3913
[7] Aumayr F, Facsko S, El-Said A S, Trautmann C and Schleberger M 2011 *J. Phys.: Condens. Matter* **23** 393001
[8] El-Said A S, Wilhelm R A, Heller R, Facsko S, Lemell C, Wachter G, Burgdörfer J, Ritter R and Aumayr F 2012 *Phys. Rev. Lett.* **109** 117602
[9] Olivares J, García G, García-Navarro A, Agulló-López F, Caballero O and García-Cabañes A 2005 *Appl. Phys. Lett.* **86** 183501
[10] Sanz R, Jensen J, Johansson A, Skupinski M, Possnert G, Boman M, Hernandez-Vélez M, Vazquez M and Hjort K 2007 *Nanotechnology* **18** 305303

[11] Krasheninnikov A V and Nordlund K 2010 *J. Appl. Phys.* **107** 071301
[12] Arnau A *et al* 1997 *Surf. Sci. Rep.* **27** 113–239
[13] Schenkel T, Hamza A V, Barnes A V and Schneider D H 1999 *Pro. Surf. Sci.* **61** 23–84
[14] Heller R, Facsko S, Wilhelm R A and Möller W 2008 *Phys. Rev. Lett.* **101** 096102
[15] Minniti R, Ratliff L P and Gillaspy J D 2001 *Phys. Scr.* **T92** 22–26
[16] El-Said A S *et al* 2008 *Phys. Rev. Lett.* **100** 237601
[17] Zhou P *et al* 2013 *Nucl. Instrum. Methods. Phys. Res.* B **307** 221–24
[18] Tona M, Watanabe H, Takahashi S, Nakamura N, Yoshiyasu N, Sakurai M, Terui T, Mashiko S, Yamada C and Ohtani S 2007 *Surf. Sci.* **01** 723–27
[19] Tona M, Fujita Y, Yamada C and Ohtani S 2008 *Phys. Rev.* B **77** 155427
[20] Terada M, Nakamura N, Nakai Y, Kanai Y, Ohtani S, Komaki K and Yamazaki Y 2005 *Nucl. Instum. Methods. Phys. Res.* B **235** 452–5
[21] Tona M *et al* 2007 *J. Phys. Conf. Ser.* **58** 331–4
[22] Ritter R, Kowarik G, Meissl W, Suss L, Maunoury L, Lebius H, Dufour C, Toulemonde M and Aumayr F 2010 *Nucl. Instum. Methods. Phys. Res.* B **268** 2897–900
[23] Ritter R, Shen Q, Wilhelm R A, Heller R, Ginzel R, López-Urrutia J R C, Facsko S, Teichert C and Aumayr F 2013 *Nucl. Instum. Methods. Phys. Res.* B **315** 252–56
[24] Ritter R *et al* 2013 *Appl Phys Lett* **102** 063112
[25] Noack M, Kölsch P, Schäfer R, Toussaint P and Caro J 2002 *Chem. Eng. Technol.* **25** 221–30
[26] Tong H D, Jansen H V, Gadgil V J, Bostan C G, Berenschot E, van Rijn C J M and Elwenspoek M 2004 *Nano. Lett.* **4** 283–87
[27] Zschornack G *et al* 2008 *Rev. Sci. Instrum.* **79** 02A703
[28] Turchanin A, Käfer D, El-Desawy M, Wöll C, Witte G and Gölzhäuser A 2009 *Langmuir* **25** 7342–52
[29] Angelova P *et al* 2013 *Acs Nano* **7** 6489–97
[30] Turchanin A, Beyer A, Nottbohm C T, Zhang X H, Stosch R, Sologubenko A, Mayer J, Hinze P, Weimann T and Gölzhäuser A 2009 *Adv. Mater.* **21** 1233–7
[31] Wilhelm R A, Gruber E, Ritter R, Heller R, Facsko S and Aumayr F 2014 *Phys. Rev. Lett.* **112** 153201
[32] Bodewits E, Hoekstra R, Dobes K and Aumayr F 2014 *Phys. Rev.* A **90** 052703
[33] Biersack J 1993 *Nucl. Instrum. Methods. Phys. Res.* B **8081** 12–15
[34] Ritter R *et al* 2012 *Europhys. Lett.* **97** 13001